RESEARCH PAPER

Experimental study on the velocity-dependent frictional resistance of a rough rock fracture exposed to normal load vibrations

Wengang Dang[1,2,3] · Junpeng Chen[1] · Linchong Huang[3,4]

Abstract

Changes in shear velocity can strengthen or weaken the frictional resistance of joints/faults in natural systems, but the mechanism remains unclear. We investigated the shear behavior of a rough basalt fracture in well-controlled, repeatable shear tests under constant and dynamic normal load conditions at different shear velocities. Normal load vibrations, simulating a dynamic normal load, were applied to the upper block of a fractured basalt sample. Simultaneously, a shear load was applied to the bottom block, providing a constant shear velocity. The peak shear strength increased with increasing shear velocity under constant normal load conditions. The peak shear strength decreased at a lower shear velocity under normal load vibrations. When the shear velocity exceeded the critical value, v_c, the peak shear strength increased. The apparent coefficient of friction reduced under normal load vibrations. The reduction in the dynamic coefficient of friction increased with increasing shear velocity. We identified a phase shift between the peak normal load and peak shear load with peak shear load delay (D1) and a phase shift between peak normal load and the peak coefficient of friction with the peak coefficient of friction delay (D2). D1 and D2 were dependent on the quasi-static coefficient of friction and shear velocity, and both decreased with increasing shear velocity. D1 decreased with the increasing quasi-static coefficient of friction, while D2 was almost constant with changes in the quasi-static coefficient of friction. A new shear strength criterion was proposed for a rough joint under a constant shear velocity and normal load vibrations.

Keywords Dynamic normal load · Friction coefficient · Phase shift · Rock mechanics · Velocity effect

✉ Wengang Dang
  dangwg@mail.sysu.edu.cn

✉ Linchong Huang
  hlinch@mail.sysu.edu.cn

  Junpeng Chen
  871120966@qq.com

1 School of Civil Engineering, Sun Yat-Sen University,
   Zhuhai 519082, People's Republic of China

2 State Key Laboratory of Coal Resources and Safe Mining,
   China University of Mining and Technology, No. 1
   University Road, Xuzhou 221116, Jiangsu, People's Republic
   of China

3 Southern Marine Science and Engineering Guangdong
   Laboratory, Zhuhai 519082, People's Republic of China

4 School of Aeronautics and Astronautics, Sun Yat-Sen
   University, Shenzhen 518107, People's Republic of China

1 Introduction

Rock masses are always jointed and anisotropic [1–3] and are commonly subjected to a dynamic loading (e.g., human activities, earthquakes, and earth tides) in natural systems [4–8]. Understanding the mechanical behaviors and failure mechanisms of joints/faults under complex load conditions is very important for the design of underground excavations, slopes, dam foundations, and geothermal reservoirs [9–13].

The variable load caused by blasting, earth tides, and earthquakes is a very complex dynamic event, where dynamic excitations occur in various directions [4, 7, 8]. In several circumstances, the shear load and normal load on surrounding faults can be changed and slip can occur along rock fractures under a variable normal load [4, 7]. To explore the frictional behavior of rock fractures under variable normal load conditions during shearing, shear tests under constant/dynamic normal load conditions are

commonly performed [14–27]. According to the different dynamic loading patterns, these tests can be divided into two categories of instantaneous/sudden changes in normal loads or continues changes in normal loads.

For an instantaneous/sudden change in the normal load, step increase tests, step decrease tests, and normal load pulse tests are typically performed. The analysis of transient effects is always the main task during data analysis. It is widely accepted that the dynamic normal load weakens the frictional resistance of faults in natural systems, and the changes in the friction with the step changes in normal forces follow a multi-stage evolution. Hobbs and Brady [14] conducted direct shear tests on gabbro exposed to changes in normal loads, in which a large instantaneous change in shear force was initially observed, followed by a time-dependent exponential process. Olsson [15] performed similar tests on welded tuff, where an immediate steep linear response was initially identified, followed by an exponential time-dependent process. Linker and Dieterich [17] investigated the frictional response to stepwise changes in normal loads on Westerly granite using a double direct shear device. They observed a three-stage shear force changing pattern, with an instantaneous increase first, followed by an immediate linear increase with time or load point displacement, and finally reaching a steady state (shear force moved toward a constant value). Hong and Marone [23] performed similar tests on quartz, lay-quartz, and Westerly granite, where the coefficient of friction changed with sudden changes in normal stress, with a three-stage frictional response observed. Kilgore et al. [24, 25] studied the frictional responses under sudden changes in normal loads on a dry bare granite surface, using a double direct shear apparatus. They found that sudden changes in normal loads lead to gradual, almost exponential changes, in shear forces. Moreover, Linker and Dieterich [17], Richardson and Marone [18], Prakash and Clifton [26], Prakash [27], and Bureau et al. [28] reported that there was memory dependence in the variations of normal loads.

Preliminary investigations of the continuous changes in normal forces on the resistance to sliding have been performed by Candela et al. [7], Dang et al. [19–22], Perfettini et al. [29], Cochard et al. [30], Boettcher and Marone [31], and Tang and Wong [32]. In these tests, the dynamic normal load was controlled by a sinusoidal wave. A distinct phase shift between peak normal force and peak shear force, with peak shear force lagging behind, was reported by Boettcher and Marone [31] and Dang et al. [20]. The phase shift was found to be dependent on shear velocity, normal load vibration amplitude, and vibration frequency. Dang et al. [20, 22] also proved that the traditional Mohr–Coulomb shear strength criterion overpredicts the peak shear strength under normal load vibrations, and they proposed a new shear strength criterion to predict the shear strength under cyclic normal load conditions. The laboratory test results were well fitted by the new shear strength criterion, which contained the phase shift.

The effects of shear velocity on shear strength have also been investigated [21, 23, 33–35]. Most studies have focused on the shear velocity effects under constant normal load conditions. An increase in shear velocity can increase or decrease the shear strength depending on the type of material [34]. Dang et al. [21], Hong and Marone [23], and Cochard and Rice [35] investigated the shear velocity effect on friction strength under dynamic normal load conditions. Shear strength does not change systematically with shear velocity under sudden changes in the normal force [23], although shear strength increases significantly with an increase in shear velocity under continuous changes in normal load [21].

In general, natural faults/joints have rough surfaces. Only under very unusual and idealized situations is a fault surface flat. However, due to the complexity and unrepeatability of shear tests on rough faults, most previous investigations of dynamic frictional behavior have focused on planer flat fault surfaces. For flat fault/joint surfaces, the coefficient of friction and the dilatancy are nearly constant at the stable shearing stage. The lack of consideration of the roughness of faults/joints has prevented a deeper understanding of the real dynamic frictional behavior. It is also possible that the shear velocity effect is different on rough faults than on flat faults.

In this study, we conducted laboratory tests on a rough basalt rock fracture to investigate the frictional resistance under constant/variable normal loads at different shear velocities. The shear tests were repeated on one sample under a smaller normal load condition. We found that the quasi-static and dynamic coefficients of friction were different. Frictional resistance was weakened under normal load vibrations. The reduction in the dynamic coefficient of friction increased with increasing shear velocity. Moreover, we observed a phase shift between peak normal load and peak shear load and a phase shift between peak normal load and the peak coefficient of friction. Our results indicated that a slow slip or creep can easily cause faults to slide under variable normal loads.

2 Laboratory tests

2.1 Apparatus and samples

The shear experiments were performed using a large servo-controlled shear box apparatus (Fig. 1a) at a room temperature of about 20 °C. The shear box apparatus consisted of both a vertical and horizontal hydraulic loading system.
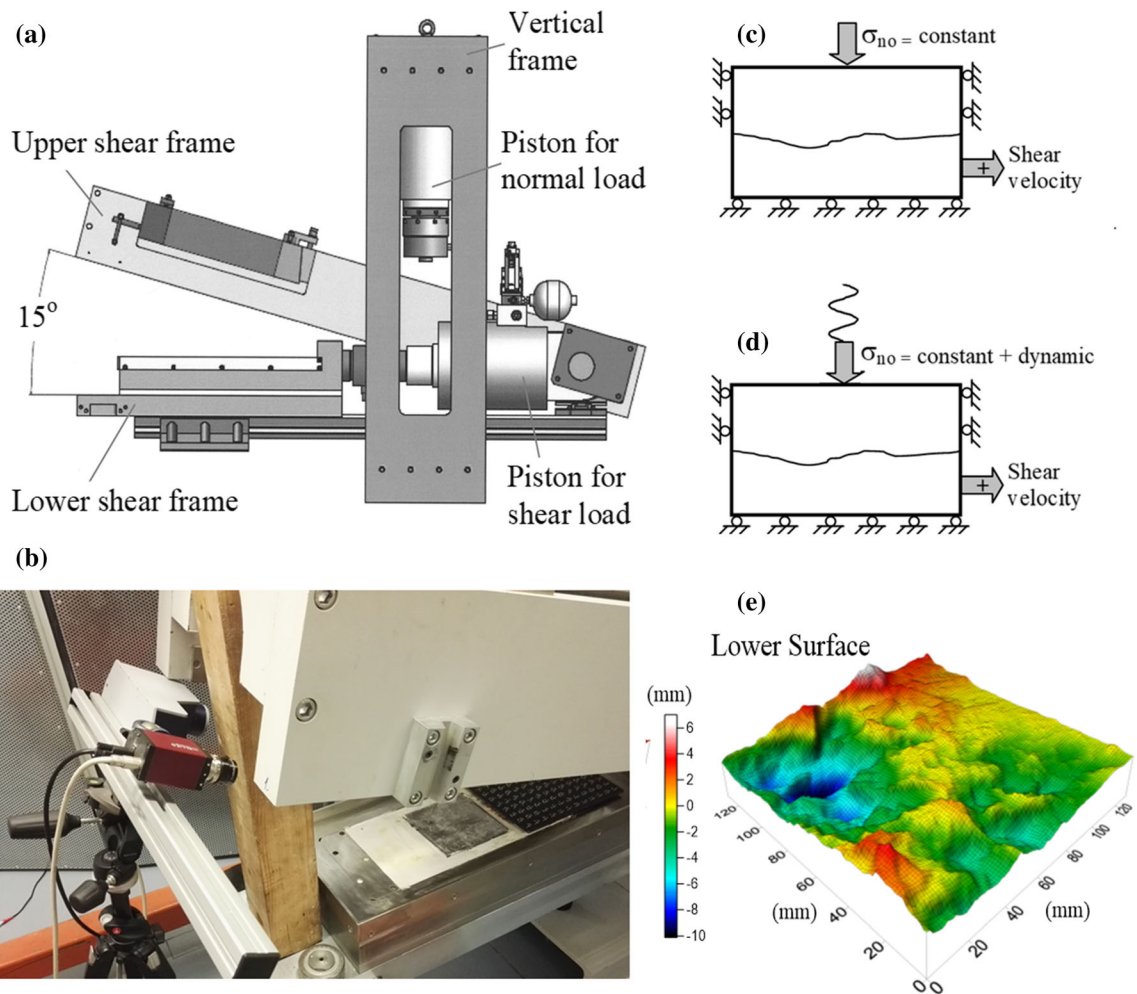
Fig. 1 Testing apparatus and experimental configuration: **a** main components of the GS-1000 shear box device; **b** the bottom block of the sample, with the 3D scanner; direct shear tests under **c** constant normal load and **d** dynamic normal load conditions; and **e** digitized fracture surface obtained from 3D scanning

The vertical piston provided constant and superimposed dynamic normal loads, with 0.1 kN resolution. The horizontal piston drove the lower shear box, with a constant shear velocity in a displacement feedback mode. Displacements and forces were measured by linear variable differential transformers (LVDTs) and load cells, respectively. Normal load, shear load, normal displacement, and shear displacement were recorded continuously 100 times/s.

In this study, experiments were performed on a rough basalt rock fracture, which had a block size of $150 \times 150 \times 100$ mm^3 (length × width × height). A rough fracture was created at a height of 50 mm. Before the shear tests, the rough surface of the upper and lower blocks was scanned using a 3D scanner (Figs. 1b and 1e). The upper surface was almost completely matched with the lower surface. Uniaxial compressive tests and Brazilian tests on samples of the same material revealed a uniaxial

compressive strength of 220 MPa, tensile strength of 16 MPa, Poisson's ratio of 0.25, and Young's modulus of 105 GPa.

2.2 Laboratory test setup

To ensure that the same rough surface could be used during each test, a small normal load was selected, which guaranteed that the large asperities of the surface were kept intact. Two types of direct shear tests were arranged into three groups, with a total of 12 tests actually performed. The first type was a direct shear test under constant normal load conditions (Fig. 1c), where the constant normal load was 50 kN, the shear velocity varied from 1 to 100 mm/min, and the maximum shear displacement was 5.0 mm. The second type was a direct shear test under variable normal load conditions (Fig. 1d), where the constant normal load varied from 40 to 50 kN, the shear velocity varied

from 1 to 100 mm/min, and the maximum shear displacement was 5.0 mm. The superimposed dynamic normal load (F_{sd}) was controlled by an external dynamic signal (Eq. 1, a sinusoidal wave), where the amplitude of the superimposed dynamic normal load (F_d) was 20/25 kN, with the normal load frequency (f) ranging from 0.5 to 1.0 Hz. The specific test scheme is documented in Table 1.

$$F_{sd} = F_d sin(2\pi ft) \tag{1}$$

The root-mean-square slope of fracture profile, Z_2, and joint roughness coefficient, JRC, were used to describe fracture surface roughness [36].

$$Z_2 = \left[\frac{1}{(n-1)(\Delta x)^2} \sum_{i=1}^{n-1} (Z_{i+1} - Z_i)^2 \right]^{\frac{1}{2}} \tag{2}$$

$$JRC = 32.2 + 32.47 log Z_2 \tag{3}$$

Based on Eqs. 2 and 3, before the test, Z_2 and JRC values are 0.260 and 13.2; after the test, Z2 and JRC values are 0.257 and 13.0 According to the shear strength law of Barton and Choubey [37], the degradation of the magnitude of JRC is small and has therefore only little influence on the shear strength.

3 Laboratory test results

3.1 Test results under constant normal load conditions

The experimental results of the direct shear test CNL-1 are shown in Fig. 2. Detailed measurements of the effect of shear velocity on frictional resistance were performed for five velocity levels of 1.0, 10, 25, 50, and 100 mm/min,

respectively. Figure 2 shows that there was no significant distinction in the test results when the shear velocity was over 25 mm/min. The peak shear load increased with increasing shear velocity, while the dilation decreased slightly with increasing shear velocity.
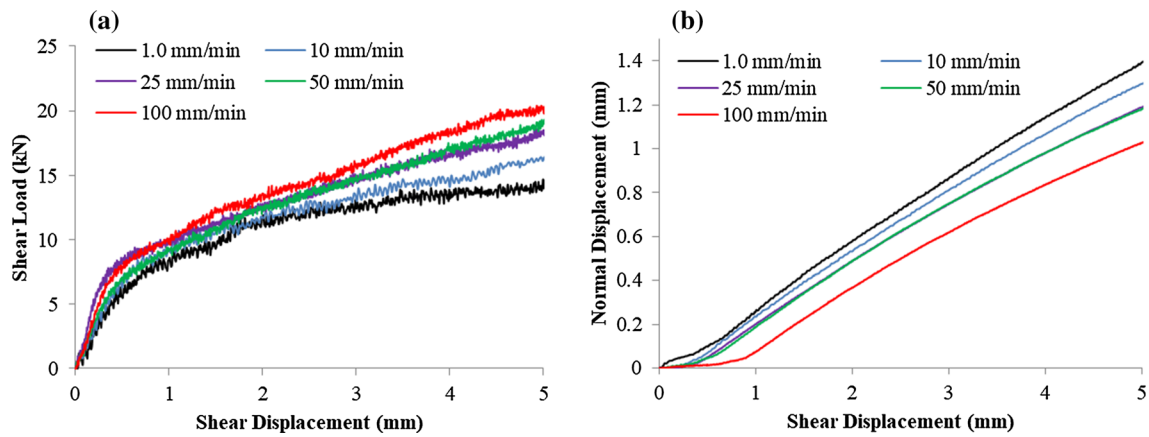
3.2 Test results under normal load vibrations

3.2.1 Changes of normal load, shear load, friction coefficient, and normal displacement

The test results under normal load vibrations are shown in Figs. 3 and 4. As shown in Fig. 3, an increase/decrease in normal load produced an increase/decrease in the shear load and coefficient of friction, while the dilation increased/decreased with a decrease/increase in normal load. Figure 4 shows the changes in the normal load, shear load, coefficient of friction, and normal displacement at different shear velocities. The velocity effect differed from that under constant normal load conditions. Within a certain amount of shear displacement, a smaller shear velocity led to a greater periodic change in the density of normal load, shear load, coefficient of friction, and normal displacement. The peak shear load was more than twice as large at the shear velocity of 100 mm/min than that at the shear velocity of 1 mm/min. An increase in shear velocity led to an increase in peak shear load, while the valley values of shear load remained almost constant and were located at the point of the minimum normal load. The peak coefficient of friction was almost the same at different shear velocities. An increase in the shear velocity led to an increase in the valley values of the coefficient of friction during each cycle. The peak coefficient of friction was almost the same as the static coefficient of friction. Shear

Table 1 Experimental program of direct shear tests under various constant normal load (CNL) and dynamic normal load (DNL) conditions

| Test	Series	Constant normal load (kN)	Dynamic normal load (kN)	Frequency of normal load change (Hz)	Maximum shear displacement (mm)	Shear velocity (mm/min)
CNL-1	1	50	-	-	5	1
	2	50	-	-	5	10
	3	50	-	-	5	25
	4	50	-	-	5	50
	5	50	-	-	5	100
DNL-1	1	40	20	0.5	5	5
	2	50	25	0.5	5	5
DNL-2	1	50	25	1	5	1
	2	50	25	1	5	10
	3	50	25	1	5	25
	4	50	25	1	5	50
	5	50	25	1	5	100

Fig. 2 Experimental results of the direct shear test CNL-1: **a** the shear load and **b** normal displacement under a constant normal load of 50 kN as a function of shear displacement at shear velocities of 1, 10, 25, 50, and 100 mm/min
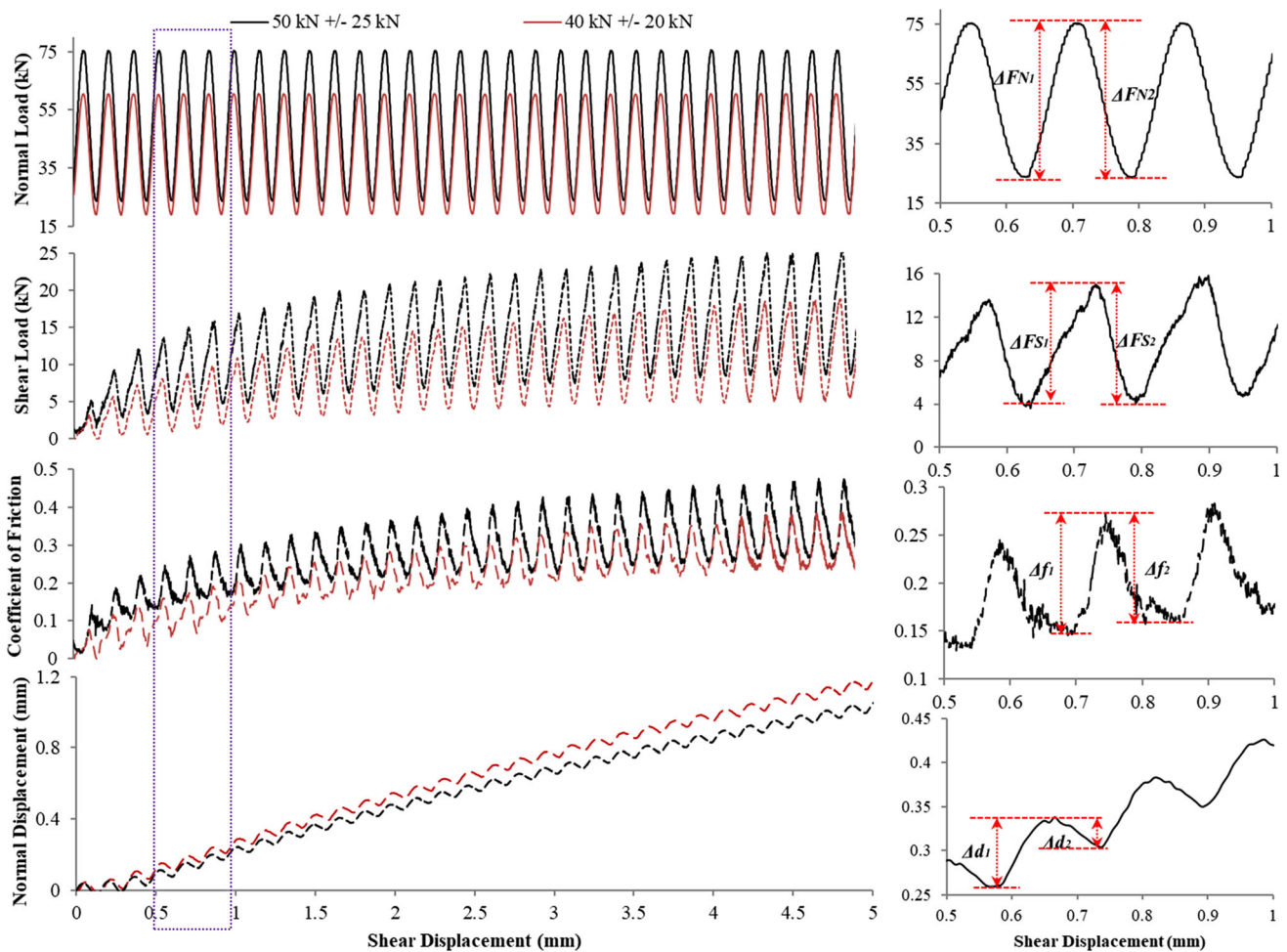
Fig. 3 Experimental results of the direct shear test DNL-1: normal load, shear load, coefficient of friction, and normal displacement as a function of shear displacement under different combinations of constant (40/50 kN) and dynamic (20/25 kN) normal loads at a shear velocity of 5 mm/min

velocity had little influence on the dilation, which had a tendency to reduce slightly with increasing shear velocity. A larger normal load led to a larger coefficient of friction

and a smaller dilation. The cyclic changes in the shear load and coefficient of friction were more serrated than sinusoidal. This velocity-dependent mechanical behavior of
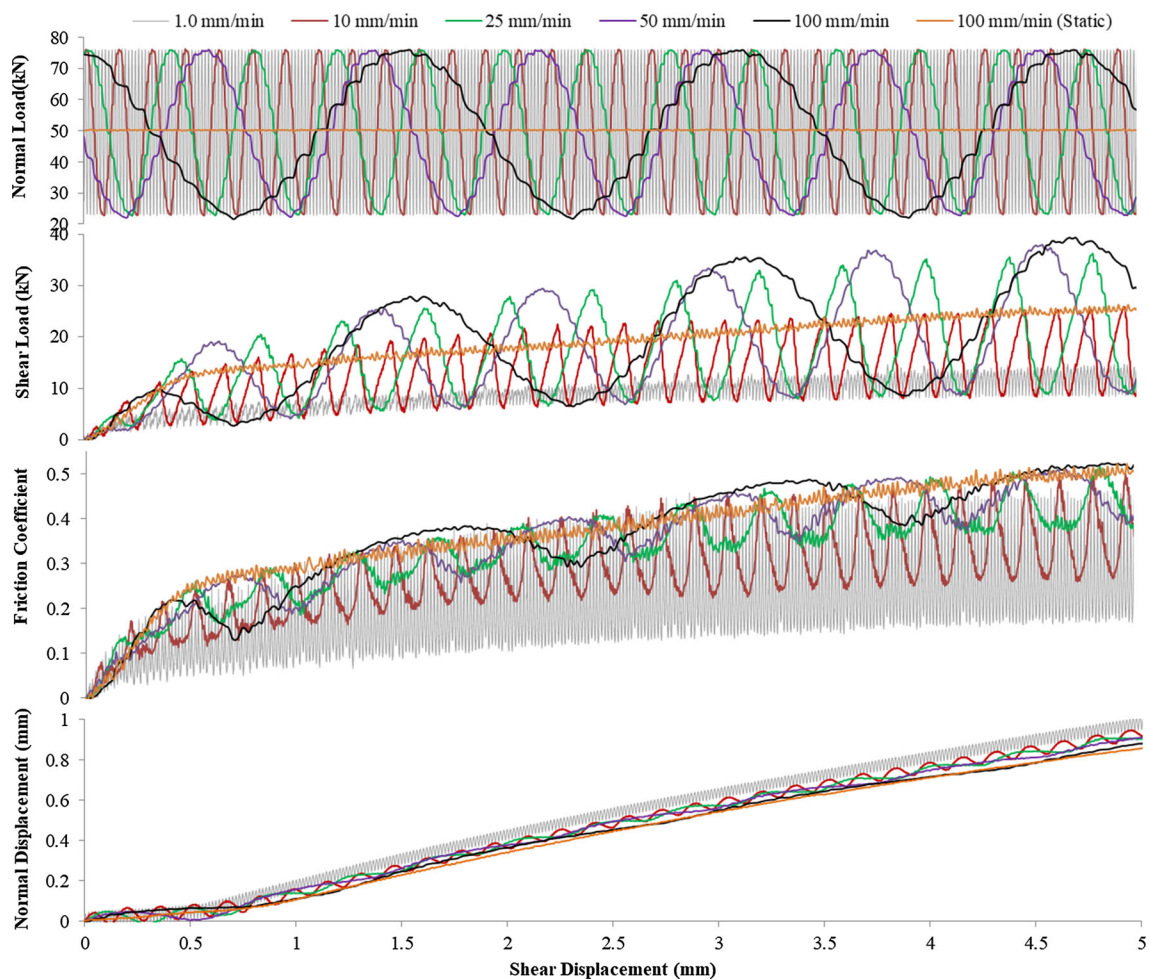
Fig. 4 Experimental results of the direct shear test DNL-2: normal load, shear load, coefficient of friction, and normal displacement as a function of shear displacement under the combination of constant (50 kN) and dynamic (25 kN) normal loads at shear velocities of 1, 10, 25, 50, and 100 mm/min

rock fractures was very different to the test results obtained under constant normal load conditions [21, 38].

Due to the changes in normal load being controlled by Eq. 1, $\Delta F_{N1} = \Delta F_{N2}$ for all the changing cycles (Fig. 4). With increasing shear displacement, the changes in shear load (ΔF_{s1} and ΔF_{s2}) gradually increased, finally reaching a constant value, where ΔF_{s1} was almost identical to ΔF_{s2}. It should be noted that ΔF_{s1} was larger than ΔF_{s2} in each cycle at the early stage. As shown in Fig. 5, the scale of the changes in shear load increased as the quasi-static coefficient of friction and shear velocity increased at both the loading and unloading stages. The ratio between the scale of the changes in shear load and the changes in normal load, i.e., $\Delta F_{s1}/\Delta F_{N1}$, had a linear relationship with the quasi-static coefficient of friction (Fig. 5c). The actual coefficient of friction followed the same pattern of variation as the shear load, which changed cyclically with the variation in the normal load. The scale of the change in the coefficient of friction increased step by step to a constant

value, where $\Delta f_{s1} = \Delta f_{s2}$. Δf_{s1} was also larger than Δf_{s2} in the early stage. The ratio between the changes in the dynamic coefficient of friction and quasi-static coefficient of friction, i.e., $\Delta f_{\text{-}dynamic}/f_{\text{-}static}$, was constant at the same shear velocity and $\Delta f_{\text{-}dynamic}/f_{\text{-}static}$ increased with increasing shear velocity (Fig. 5d). The changes in the normal displacement were in phase with the changes in normal load. In the loading stage, the dilation was inhibited, only surface asperity promoted dilation, and Δd_1 was larger than Δd_2 for all the changing cycles, where Δd_1 was located in the unloading stage and Δd_2 was located in the loading stage. The patterns of variation of shear load and the coefficient of friction were different from the previous results reported by Linker and Dieterich [17], Hong and Marone [23], and Dang et al. [20–22]. The most important reason for this was that the roughness of the contact surface was not taken into consideration in these studies.
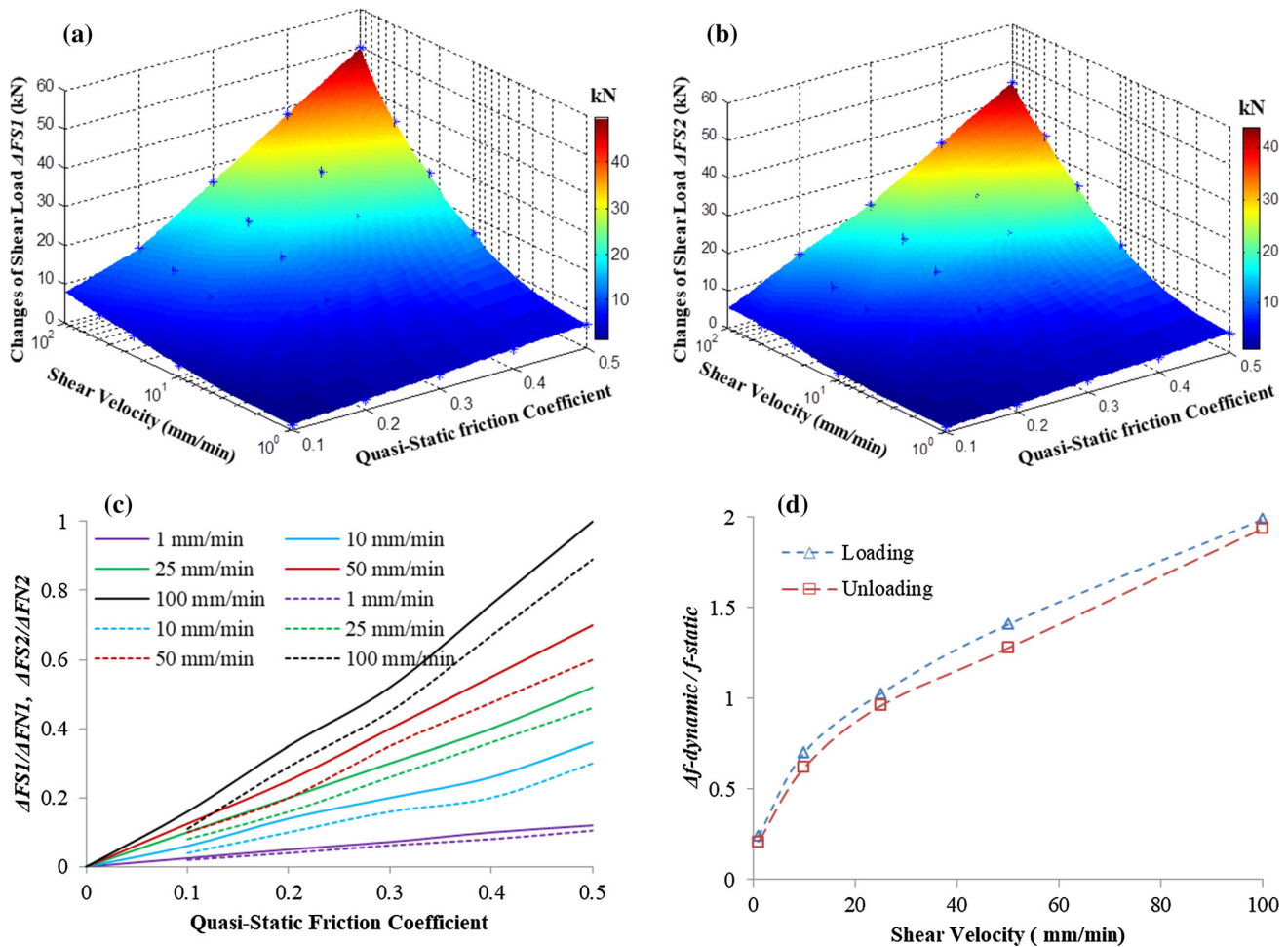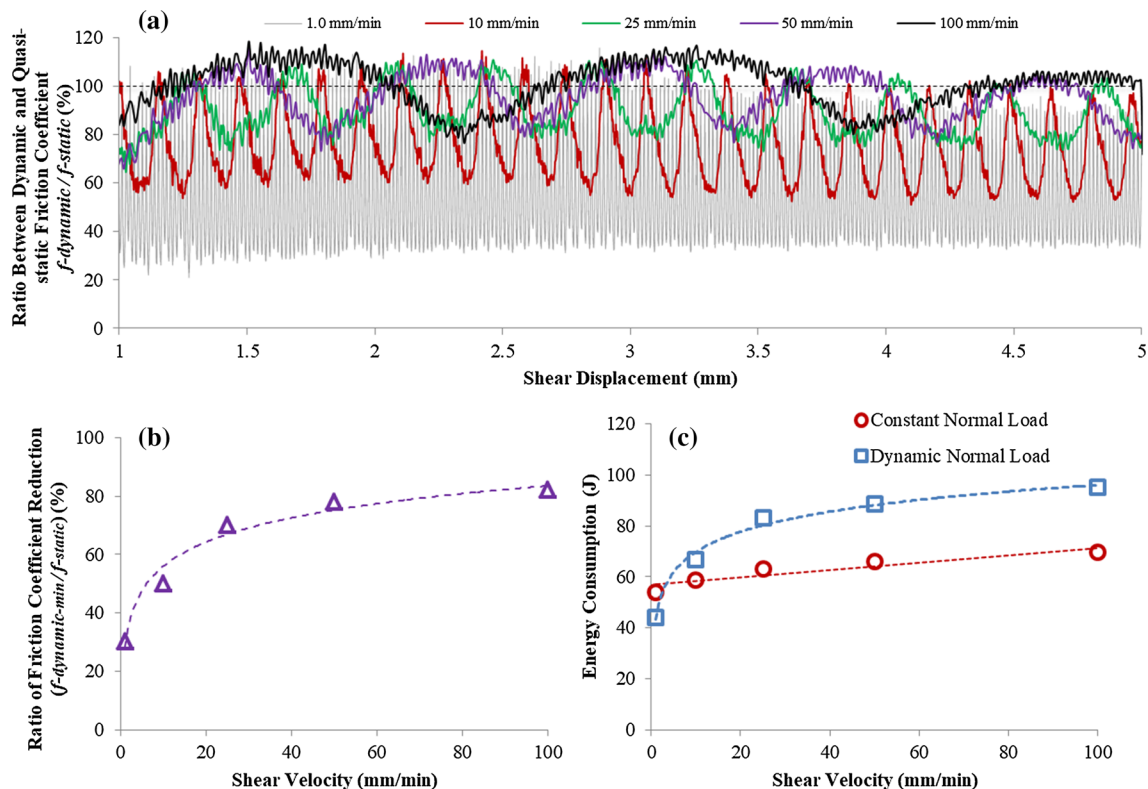
Fig. 5 Experimental results showing the **a** scale of the changes in shear load ΔF_{S1} at the loading stage; **b** scale of the changes in shear load ΔF_{S2} at the unloading stage; **c** ratio between the changes in the shear load and changes in the normal load, where solid lines indicate the loading stage ($\Delta F_{S1}/\Delta F_{N1}$) and dotted lines indicate the unloading stage ($\Delta F_{S2}/\Delta F_{N2}$); and **d** ratio between the changes in the dynamic coefficient of friction and quasi-static coefficient of friction at different shear velocities and at the same shear velocity

3.2.2 Energy consumption and reduction of friction coefficient

Energy consumption can be calculated using a shear load displacement diagram, i.e., $E = \int_0^d F_{shear} ds$, where d is the shear displacement and F_{shear} is the shear load. As reported above, the peak coefficient of friction under a normal load vibration was nearly identical to the quasi-static coefficient of friction, i.e., $f_{dynamic-max} = f_{static}$, while $f_{dynamic-min}$ declined significantly. The ratio of the dynamic coefficient of friction reduction was defined as $f_{dynamic-min}/f_{static}$. Figure 6 shows the variations in $f_{dynamic}/f_{static}$, $f_{dynamic-min}/f_{static}$, and E at different shear velocities. As shown in Fig. 6a, $f_{dynamic}/f_{static}$ changed cyclically with the variation in the normal load. For a given shear velocity, the peak and valley values of $f_{dynamic}/f_{static}$ were constant, with the peak value close to 1.0 and the valley value increasing with the shear velocity. As shown in Fig. 6b, the values of $f_{dynamic-}$

$_{min}/f_{static}$ were 30%, 50%, 70%, 78%, and 82% at a shear velocity of 1, 10, 25, 50, and 100 mm/min, respectively. The above results indicated that a larger shear velocity strengthened the frictional resistance and the slow slip easily drove the rupture of faults under dynamic normal load conditions. Energy consumption increased with increasing shear velocity under both constant and dynamic normal load conditions (Fig. 6c). At a low shear velocity, more energy was consumed under constant normal load conditions than under dynamic normal load conditions, while this behavior changed when the shear velocity exceeded the critical value. (When the shear velocity was greater than 10 mm/min, more energy was consumed under normal load vibrations than under constant normal load conditions.)

Fig. 6 a Experimental results showing the ratio between the dynamic coefficient of friction and the quasi-static coefficient of friction as a function of shear displacement; **b** percentage reduction in the ratio between the dynamic coefficient of friction and the quasi-static coefficient of friction; and **c** energy consumption under constant and dynamic normal load conditions at a shear velocity of 1, 10, 25, 50, and 100 mm/min

3.2.3 Frictional strengthening and frictional weakening

It is well known that increasing shear velocity increases the shear strength for brittle rocks under constant normal load conditions. However, the velocity-dependent behavior is changed under dynamic normal load conditions. The laboratory test results showed that the difference between steady-state peak and initial levels prior to vibrations ΔF_{yield} (Fig. 7a) can be negative or positive at different shear velocities. (Negative and positive values of ΔF_{yield} indicate weakening or strengthening, respectively). The negative or positive value of ΔF_{yield} is also observed under different dynamic normal load amplitude [31]. Figure 7b shows the effect of velocity on the degree of dynamic strengthening/weakening. For the given normal load vibration amplitude, and frequency, at a lower shear velocity ΔF_{yield} was negative. The negative values became positive with increasing shear velocity until an almost constant peak value was reached. A critical shear velocity v_c was defined at the point of $\Delta F_{yield}/F_s = 0$ (shaded bar in Fig. 7b), which separated the areas of frictional weakening ($v > v_c$) and frictional strengthening ($v < v_c$).

4 Discussion

4.1 Phase shift

Perfettini et al. [29] was first who reported the phase lag between shear stress and normal stress under normal load vibrations using an analytical mathematical, i.e., equation (Eq. 4). Boettcher and Marone [31] and Dang et al. [20] observed the phase lag between peak shear force and peak normal force in the laboratory. Dang et al. [20–22] reported that the relative phase shift between peak normal load and peak shear load increases with increasing normal load, decreasing normal force impact amplitude, and decreasing shear velocity. This phase shift is caused by the shear stiffness of the fracture. The relative phase shift between peak normal load and peak coefficient of friction reported by Dang et al. [20] was almost constant at about half a cycle in all tests.

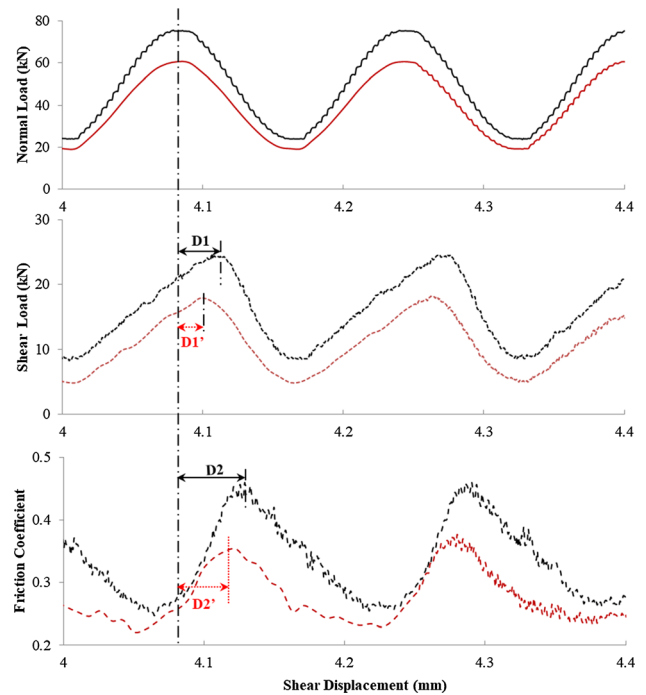$$\tau = f_{static}\sigma_n[1 + \varepsilon\rho_\tau sin(ft - \gamma_\tau)]$$

As shown in Figs. 8 and 9, the phase shift was also apparent in the present work, where the relative phase shift between peak normal load and peak shear load (D1) increased with increasing normal load and decreasing shear velocity. As shown in Fig. 8, the relative phase shift of D1
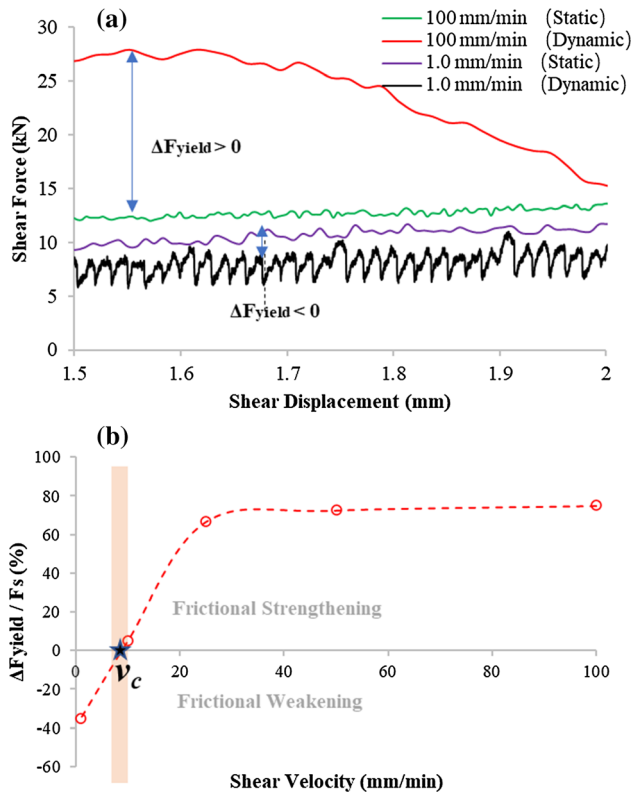
Fig. 7 Quantification of the friction response in relation to the normal load variation. **a** Change in peak yield strength (ΔF_{yield}) represented as the difference between the steady-state peak and initial level prior to vibrations. Note that ΔF_{yield} can be positive or negative, indicating induced strengthening or weakening, respectively. **b** Normalized frictional strengthening/weakening effects as a function of shear velocity. The critical shear velocity v_c was defined at the point of $\Delta F_{yield}/F_s = 0$ (shaded bar: $v < v_c$ indicates induced frictional weakening, $v > v_c$ indicates induced frictional strengthening)

Fig. 8 The phase shift D1 between the peak shear load and peak normal load, and the phase shift D2 between the peak coefficient of friction and peak normal load. The red lines denote 40 ± 20 kN and the black lines denote 50 ± 25 kN

decreased as the quasi-static coefficient of friction increased. Due to the asperities of the contact surface, the relative phase shift between peak normal load and peak coefficient of friction (D2) differed from the results reported by Dang et al. [20], with D2 decreasing with increasing shear velocity and being little influenced by the quasi-static coefficient of friction. When the shear velocity ranged from 5 to 25 mm/min, D2 decreased with increasing shear velocity, while D2 remained almost constant when the shear velocity ranged from 25 to 100 mm/min. In the phase lag law (Eq. 4) reported by Perfettini et al. [29], the phase shift is controlled by the normal stress, steady friction coefficient, modulus of normalized shear stress change, and impact frequency. Equation 2 also indicates that for periods where excitation is very low, the phase shift weakens. The law expressed in Eq. 4 was in good agreement with our result that a large shear velocity led to a smaller phase shift D1 (with the same normal load impact frequency, a larger shear velocity indicated a smaller period with a certain amount of shear displacement).

During tidal normal stress fluctuations, reservoir effects and earthquakes, the phase shift between the peak normal stress and peak shear stress may guide people to optimize the dynamic support parameters on some creeping offshore structures, reservoir dams and slops, etc. When the creeping/slipping projects under dynamic normal load, the peak shear strength can be determined and the time when the peak shear strength occur can be calculated according to the quasi-static friction coefficient, normal stress, dynamic normal load amplitude and frequency.

4.2 Shear strength prediction

Dang [20] reported that the classical shear strength criterion under constant normal load conditions overpredicts the value under dynamic normal load conditions, and they proposed a new one. However, the proposed shear strength criterion was only used for planar joints. As shown in Fig. 6a, the ratio between the actual dynamic coefficient of friction and quasi-static coefficient of friction, i.e., $f_{dynamic}/f_{static}$ followed a sinusoidal waveform. The actual dynamic coefficient of friction can be represented by the multiplication of the variables of the quasi-static coefficient of friction and sinusoidal waveform. As shown in Figs. 8 and 9, there was a constant phase shift between the peak normal load and peak coefficient of friction. The dynamic coefficient of friction can be determined by Eq. 5, where a and b
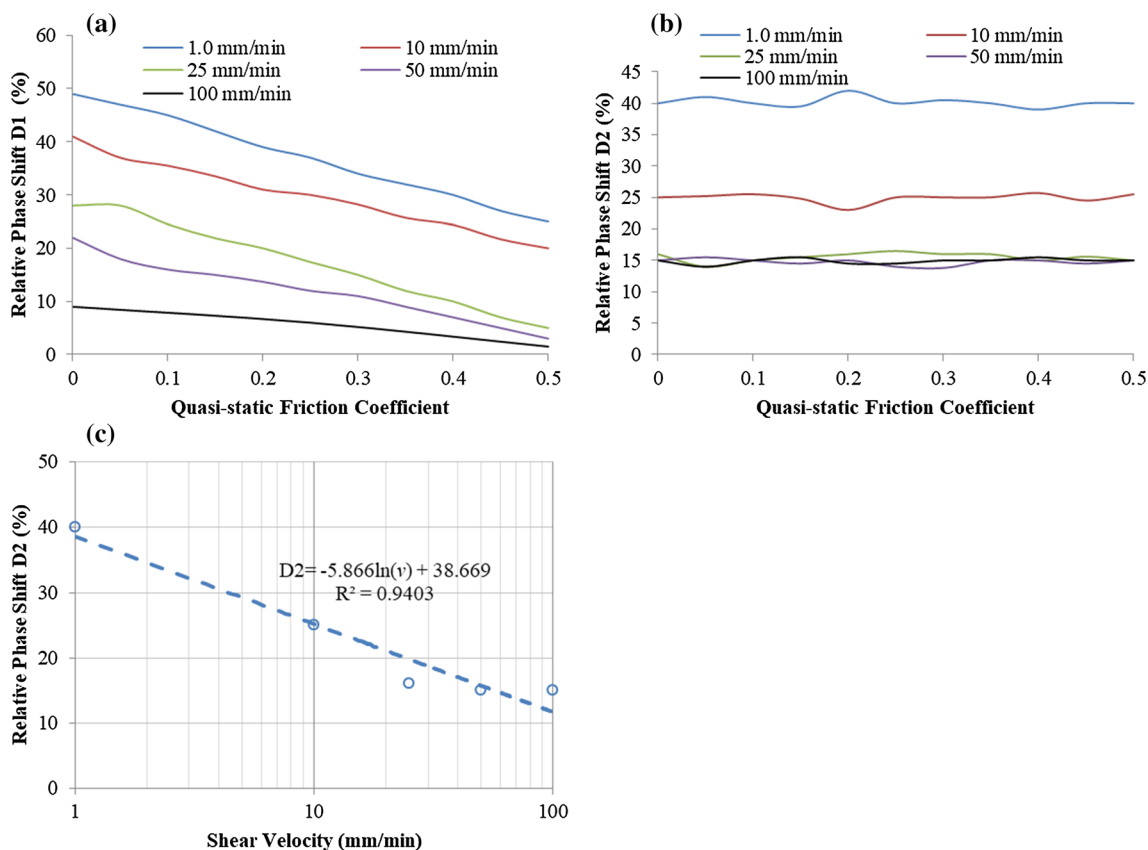
Fig. 9 **a** Relative phase shift D1 vs the quasi-static coefficient of friction, **b** relative phase shift D2 vs the quasi-static coefficient of friction, and **c** the relative phase shift D2 vs shear velocity

are the constant variables. The variable a increases, while the value of b decreases with increasing shear velocity. According to Eq. 1, the normal stress can be expressed by Eq. 6. The shear strength of the rough fault under dynamic normal load conditions can be expressed by Eq. 7. Figure 10 shows a comparison between the shear strength predicted by Eq. 7 and the laboratory test results. The values predicted by the proposed criterion were in close agreement with the measured values. The proposed shear strength prediction Eq. 7 includes the time variable, t, which can predict the shear strength at any time. However, the sinusoidal normal load is an idealized model. We consider that as a first step of investigation to understand the mechanisms of the engineering disasters (e.g., landslides, rockfall, earthquake damage etc.) under dynamic excitation [11, 40]. Future work will consider real earthquake signals instead of the standard sine waves.

$$f_{dynamic} = f_s(a + b \cdot sin(2\pi f(t + \Delta t)))\tag{5}$$

$$\sigma_n = \frac{F_s + F_d sin(2\pi ft)}{S}\tag{6}$$

$$\tau = \sigma_n f_{dynamic}$$
$$= \frac{F_s + F_d sin(2\pi ft)}{S}f_s(a + b \cdot sin(2\pi f(t + \Delta t)))\tag{7}$$

4.3 Parameter α

Linker and Dieterich [17] proposed a parameter α to quantify the changes in shear strength with changes in normal strength. The parameter α is the normalized frictional response to a normal stress step and is defined as $\alpha = (\Delta\tau/\sigma)/ln(\sigma/\sigma_0)$, where α is a constant value $(0 \leq \alpha \leq f_{static})$; $\Delta\tau$ is the transient change in shear stress; σ is the final normal stress; and σ_0 is the initial normal stress. Following Linker and Dieterich [17], Hong and Marone [23], Perfettini et al. [29], Cochard and Rice [35] and Rice et al. [39], the above equation was used to derive the value of α. However, these studies were not in complete agreement.

Hong and Marone [23] performed double shear tests on quartz, clay-quartz, and Westerly granite under variable normal loads, with different humidity levels at different shear velocities and found that α was independent of shear velocity and varied with changes in the humidity and shear
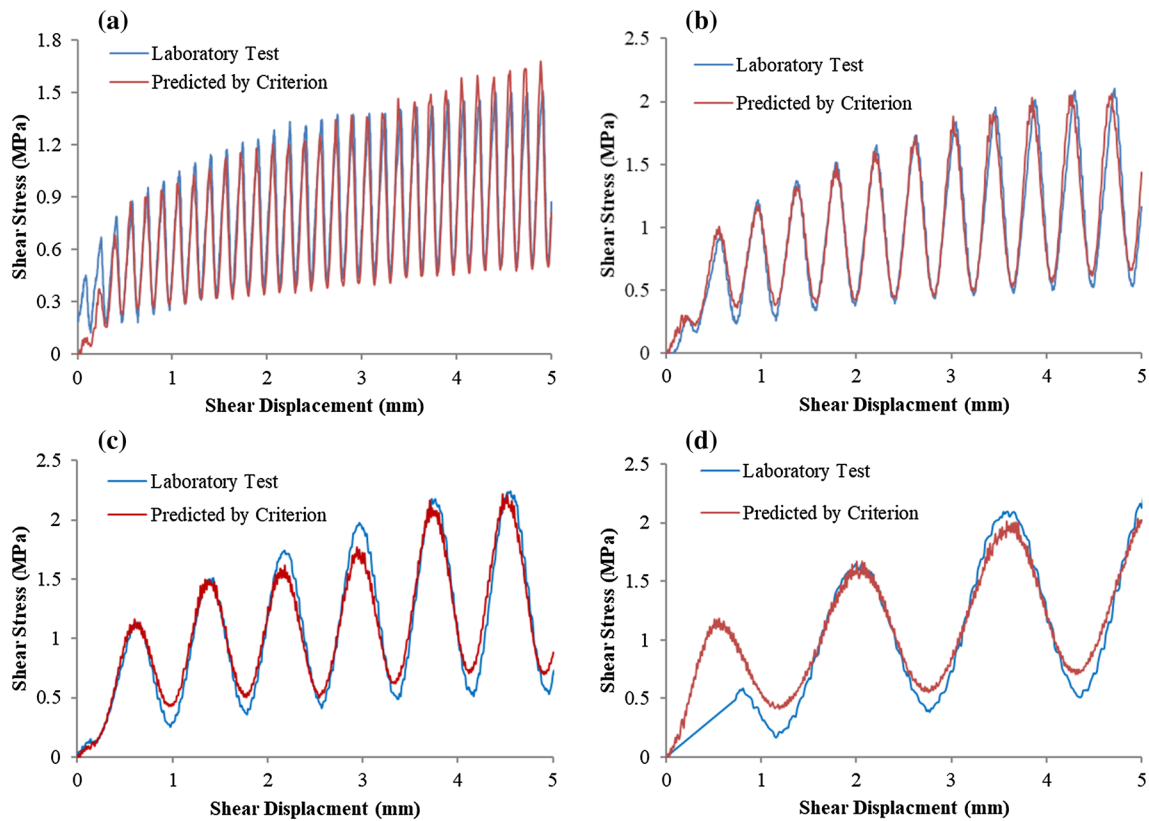
Fig. 10 Comparison of the shear stress between the laboratory test results and that predicted by the proposed shear strength criterion, **a** at a shear velocity of 10 mm/min, a = 0.8, b = 0.2; **b** at a shear velocity of 25 mm/min, a = 0.9, b = 0.1; **c** at a shear velocity of 50 mm/min, a = 0.95, b = 0.05; and **d** at a shear velocity of 100 mm/min, a = 0.99, b = 0.01

loading history. α decreased with shear displacement for gouge but not bare granite surfaces and increased with increasing humidity in quartz gouge but decreased for lay-rich gouge. Cochard and Rice [35], Perfettini et al. [29], and Rice et al. [37] reported that some test results (e.g., Bureau et al., [28]) under dynamic normal load conditions cannot be interpreted by the Linker and Dieterich law. Perfettini et al. [29] and Cochard and Rice [35] proposed that α is related to the shear velocity and the state of the asperity contacts, i.e., $\alpha = \alpha(v, \Psi)$, where v is the shear velocity and Ψ is the state of the asperity contacts.

In our tests, we focused on the periodic response rather than the transient process. As shown in Fig. 11, the changes in shear strength with changes in normal strength could also be quantified by a constant value. Here we defined a parameter β. $\beta = f(v, f\text{-static})$, where v is the shear velocity and $f\text{-static}$ is the quasi-static coefficient of friction. β could be described by Eq. 8, where $0 \leq \beta$ indicates the shear velocity approaches zero, and the larger the value of β the smaller the changes in normal load, which is to some extent similar to the law proposed by Cochard and Rice [35]. Equation 8 indicates that β is dependent on the shear velocity and quasi-static coefficient of friction.
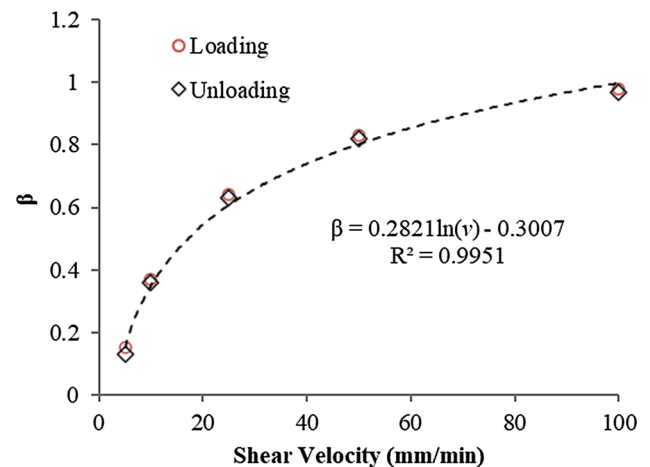
Fig. 11 β in the loading and unloading stages as a function of shear velocity

$$\beta = f(v) \frac{\Delta F_S}{\Delta F_N} / f_{static}$$

Hong and Marone [23] revealed that the peak shear strength displays a declining trend with ongoing shear displacement, which indicates a friction degradation during the experiments. Dynamic friction degradation of the

sliding surface is widely assumed [40]. We considered that the decrease in α with shear displacement should be attributed to the decrease in the coefficient of friction. We also speculated that the effect of humidity on α was related to the quasi-static coefficient of friction of the material under different levels of humidity. To summarize, for a smooth planar fault, the state of the surface contacts and the coefficient of friction were constant at the steady sliding stage, where α had a constant value. For a rough surface, the state of the asperity contacts and the coefficient of friction changed during shearing, and the Cochard and Rice [35] law was more suitable for analyzing the parameter α. We speculated that α increases with an increase in the quasi-static coefficient of friction.

After the test, the surfaces of the upper and the lower blocks were scanned again and the aperture size between the upper block and the lower block were calculated. As shown in Fig. 12, the maximum sheared off size between the upper and lower blocks was less than 2.0 mm, with the size of most apertures being less than 0.1 mm. This indicates that only the micro-asperities were sheared off and the repeated shear tests were reasonable.

5 Conclusion

Using an experimental method to investigate the dynamic frictional resistance of a rock fracture at different shear velocities, we showed that dynamic loading changes the coefficient of friction and the dilation of the upper block. The coefficient of friction weakened under dynamic normal load conditions, where the reduction in the coefficient of friction was dependent on the shear velocity. The peak shear strength increased with increasing shear velocity. The reduction in the coefficient of friction increased with increasing shear velocity. We also identified phase shifts between peak shear load and peak normal load with the peak shear load delay (D1) and between the peak coefficient of friction and peak normal load with the peak coefficient of friction delay (D2). The phase shift was dependent on the quasi-static coefficient of friction and
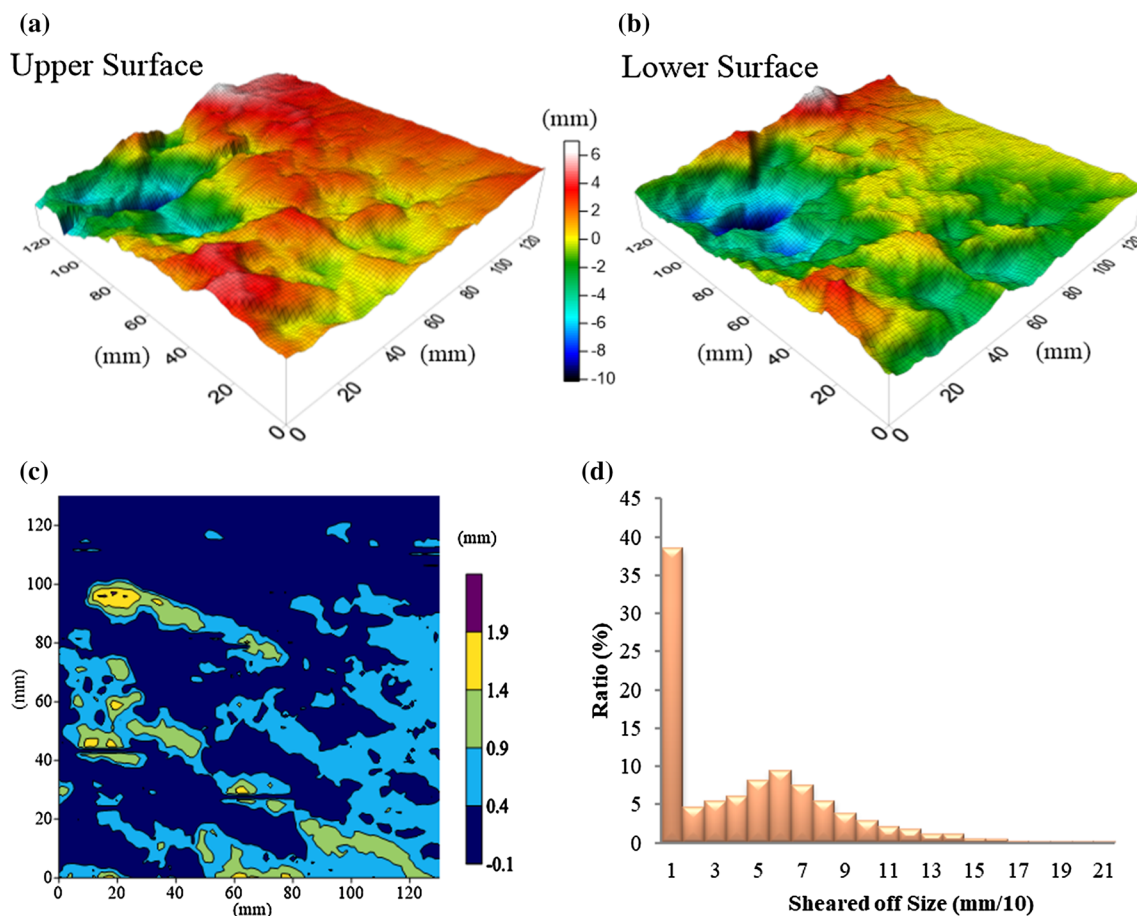
Fig. 12 After the shear test, the upper and lower blocks were scanned using the 3D scanner zSnapper. The broken area was calculated according to the coordinates of the surface in the Z direction. **a** Digitized upper surface obtained from 3D scanning after the test; **b** digitized lower surface obtained from 3D scanning after the test; **c** sheared off contour of the fracture surface; and **d** sheared off size distribution

shear velocity, where D1 and D2 had a tendency to decline with increasing shear velocity. D1 decreased with an increase in the quasi-static coefficient of friction, while D2 was almost constant with changes in the quasi-static coefficient of friction. A new shear strength criterion was proposed for a rough joint under a constant shear velocity and normal load vibrations. Our results implied that slow creep under dynamic loading should be particularly sensitive to fault slippage.

One shortcoming of all of these experiments was that the fatigue life of the fracture asperity and water effects [41–43] were not taken into consideration. Moreover, the normal load vibration frequency and vibration amplitude were not considered. In future laboratory tests, by focusing on the damage to the asperities under larger normal load conditions, the effects of normal load vibration frequency and vibration amplitude will be evaluated.

List of symbols F_s: Quasi-static normal force (kN); F_d: Dynamic normal force amplitude (kN); F_{sd}: Dynamic normal force (kN); F_{shear}: Shear force (kN); σ_n: Initial normal stress (MPa); σ: Final normal stress (MPa); τ: Shear stress (MPa); S: Nominal area of the shear plane (m^2); f: Frequency (Hz); t: Time (s); v: Shear velocity (mm/min); v_c: Critical shear velocity (mm/min); f_{static}: Coefficient of quasi-static friction, i.e., initial coefficient of friction (–); $f_{dynamic}$: Coefficient of dynamic friction (–); ΔF_N: Changes of normal force (kN); ΔF_s: Changes of shear force (kN); ΔF_{N1}: Changes of normal force in the loading stage (kN); ΔF_{N2}: Changes of normal force in the unloading stage (kN); ΔF_{s1}: Changes of shear force in the loading stage (kN); ΔF_{s2}: Changes of shear force in the unloading stage (kN); Δf_{s1}: Changes of coefficient of friction in the loading stage (–); Δf_{s2}: Changes of coefficient of friction in the unloading stage (–); Δd_1: Changes of normal displacement in the loading stage (mm); Δd_2: Changes of normal displacement in the unloading stage (mm); ΔF_{yield}: Difference of F_{shear} between steady-state peak and initial level prior to vibration (kN); $\Delta\tau$: Transient change in shear stress (MPa); Δt: Time shift (s); D1: Phase shift between peak normal force and peak shear force (–); D2: Phase shift between peak normal force and peak friction coefficient (–); a: Factor 1 (–); b: Factor 2 (–); α: Parameter 1 (–); β: Parameter 2 (–); ρ_τ: Modulus of the normalized shear stress change (–); γ_τ: Phase shift (°); E: Energy consumption (J); d: Shear displacement (mm); Ψ: State of the asperity contacts (–)

Compliance with ethical standards

References

1. Li Y, Sun S, Tang C (2019) Analytical prediction of the shear behaviour of rock joints with quantified waviness and unevenness through wavelet analysis. Rock Mech Rock Eng 52:1–13

2. Shang J, West LJ, Hencher SR (2018) Tensile strength of large-scale incipient rock joints: a laboratory investigation. Acta Geotech 13:869–886

3. Dang W, Konietzky H, Frühwirt T (2016) Rotation and stress changes of a plane joint during direct shear tests. Int J Rock Mech Min Sci 89:129–135

4. Stein RS (1999) The role of stress transfer in earthquake occurrence. Nature 402:605–609

5. Du HB, Dai F, Xu Y, Wei MD (2020) Mechanical responses and failure mechanism of hydrostatically pressurized rocks under combined compression-shear impacting. Int J Mech Sci 165:105219

6. Adam C, Adam D, Kopf F, Paulmichl I (2009) Computational validation of static and dynamic plate load testing. Acta Geotech 4(1):35–55

7. Candela T, Brodsky EE, Marone C, Elsworth D (2014) Laboratory evidence for particle mobilization as a mechanism for permeability enhancement via dynamic stressing. Earth Planet Sci Lett 392:279–291

8. Julian BR (2000) Period doubling and other nonlinear phenomena in volcanic earthquakes and tremor. J Volcanol Geothermal Res 101(1):19–26

9. Eshiet KI, Sheng Y (2017) The role of rock joint frictional strength in the containment of fracture propagation. Acta Geotech 12:897–920

10. Huang D, Song Y, Cen D (2016) Numerical modeling of earthquake-induced landslide using an improved discontinuous deformation analysis considering dynamic friction degradation of joints. Rock Mech Rock Eng 49(12):1–20

11. Huang D, Li Y, Song Y, Xu Q, Pei X (2019) Insights into the catastrophic Xinmo rock avalanche in Maoxian county, China: combined effects of historical earthquakes and landslide amplification. Eng Geol 258:105158

12. Wu H, Zhao G, Liang W (2019) Investigation of cracking behavior and mechanism of sandstone specimens with a hole under compression. Int J Mech Sci 163:105084

13. Cao W, Li X, Tao M (2016) Vibrations induced by high initial stress release during underground excavations. Tunn Undergr Space Technol 53:78–95

14. Hobbs BE, Brady BHG (1985) Normal stress changes and the constitutive law for rock friction (abstract). Eos Trans AGU 66:385

15. Olsson WA (1988) The effects of normal stress history on rock friction, key questions in rock mechanics, in Proceedings of the 29th U.S. Symposium, edited by P. A. Cundall, R. L. Sterling, and A. M. Starfield, 111–117, Univ. of Minnesota, Balkema.

16. Konietzky H, Frühwirt T, Luge H (2012) A new large dynamic rock mechanical direct shear box device. Rock Mech Rock Eng 45(3):427–432

17. Linker MF, Dieterich JH (1999) Effects of variable normal stress on rock friction: Observations and constitutive equations. J Geophys Res 97:4923–4940

18. Richardson E, Marone C (1999) Effects of normal force vibrations on frictional healing. J Geophys Res 28:859–878

19. Dang W, Konietzky H, Frühwirt T, Herbst M (2020) Cyclic frictional responses of planar joints under cyclic normal load conditions: Laboratory tests and numerical simulations. Rock Mech Rock Eng 53:337–364

20. Dang W, Konietzky H, Frühwirt T (2016) Shear behaviour of a plane joint under dynamic normal load (DNL) conditions. Eng Geol 213:133–141

21. Dang W, Konietzky H, Chang L, Frühwirt T (2018) Velocity-frequency-amplitude-dependent frictional resistance of planar joints under dynamic normal load (DNL) conditions. Tunn Undergr Space Technol 79:27–34

22. Dang W, Konietzky H, Frühwirt T (2017) Direct shear behavior of planar joints under cyclic normal load conditions: effect of different cyclic normal force amplitudes. Rock Mech Rock Eng 50(4):1–7

23. Hong T, Marone C (2005) Effects of normal stress perturbations on the frictional properties of simulated faults. Geochem Geophys Geosyst 6:Q03012

24. Kilgore B, Beeler N, Lozos JD (2017) Rock friction under variable normal stress. J Geophys Res Solid Earth 122:1–34

25. Kilgore B, Lozos J, Beeler N, Oglesby D (2012) Laboratory observations of fault strength in response to changes in normal stress. J Appl Mech 791007.

26. Prakash V, Clifton RJ (1993) Time resolved dynamic friction measurements in pressure-shear, in Experimental Techniques in the Dynamics of Deformable Solids. Appl Mech Div ASME 165:33–48

27. Prakash V (1998) Frictional response of sliding interfaces subjected to time varying normal pressures. J Tribol 120:97–102

28. Bureau L, Baumberger T, Caroli C (2000) Shear response of a frictional interface to a normal load modulation. Phys Rev E Stat Phys Plasmas Fluids Relat Interdiscip Topics 62(5):6810–6820

29. Perfettini H, Schmittbuhl J, Rice JR, Cocco M (2001) Frictional response induced by time dependent fluctuations of the normal loading. The analysis of international relations. Prentice Hall J Geophys Res 106:455–472

30. Cochard A, Bureau L, Baumberger T (2003) Stabilization of frictional sliding by normal load vibrations. J Appl Mech 70:220–226

31. Boettcher MS, Marone C (2004) Effects of normal stress variation on the strength and stability of creeping faults. J Geophys Res Solid Earth 109(B3).

32. Tang ZC, Wong LNY (2016) Influences of normal loading rate and shear velocity on the shear behavior of artificial rock joints. Rock Mech Rock Eng 49(6):1–8

33. Beeler NM, McLaskey G, Lockner D, Kilgore B (2019) Near-fault velocity spectra from laboratory failures and their relation to natural ground motion. J Geophys Res Solid Earth JB017638.

34. Crawford AM, Curran JH (1981) The influence of shear velocity on the frictional resistance of rock discontinuities. Int J Rock Mech Min Sci Geomech Abstracts 18(6):505–515

35. Cochard A, Rice JR (2000) Fault rupture between dissimilar materials: Ill-posedness, regularization, and slip-pulse response. J Geophys Res 105:891–925

36. Tse R (1979) Cruden DM (1979) Estimating joint roughness coefficients. Int J Rock Mech Min Sci Geomech Abstr 16(5):303–307

37. Barton NR, Choubey V (1977) The shear strength of rock joints in theory and practice. Rock Mech 10:1–54

38. Wang G, Zhang X, Jiang Y, Wu X, Wang S (2016) Rate-dependent mechanical behavior of rough rock joints. Int J Rock Mech Min Sci 83:231–240

39. Rice JR, Lapusta N, Ranjith K (2001) Rate and state dependent friction and the stability of sliding between elastically deformable solids. J Mech Phy Solid 49:1865–1898

40. Song Y, Huang D, Cen D (2016) Numerical modelling of the 2008 Wenchuan earthquake-triggered Daguangbao landslide using a velocity and displacement dependent friction law. Eng Geol 215:50–68

41. Dang W, Wu W, Konietzky H, Qian J (2019) Effect of shear-induced aperture evolution on fluid flow in rock fractures. Comp Geotech 114:103152

42. Song Z, Konietzky H, Herbst M (2018) Bonded-particle model-based simulation of artificial rock subjected to cyclic loading. Acta Geotech 14:955–971

43. Cai X, Zhou Z, Du X (2020) Water-induced variations in dynamic behavior and failure characteristics of sandstone subjected to simulated geo-stress. Int J Rock Mech Min Sci 130:104339

Publisher's Note Springer Nature remains neutral with regard to jurisdictional claims in published maps and institutional affiliations.